ATLAS Latest Results

F. Dittus[a], on behalf of the ATLAS Collaboration

[a]European Organization for Nuclear Research, CERN, CH-1211 Geneva 23, Switzerland

First results from the analysis of proton-proton collisions recorded with the ATLAS detector at the LHC are presented. The data sets analyzed were collected at centre-of-mass energies of 900 GeV and 7 TeV using a minimum-bias trigger, and correspond to varying integrated luminosities up to $\sim$9 μb^{-1} and $\sim$8 nb^{-1}, respectively.

ATL-GEN-PROC-2010-009
25 August 2010

1. INTRODUCTION

The Large Hadron Collider (LHC) at CERN provided stable colliding beams at $\sqrt{s} = 900$ GeV for the first time in December 2009, and at $\sqrt{s} = 7$ TeV on March 30, 2010. Good performance of the ATLAS Detector has been readily seen with the first collision data, as reported in ref. [1]. An overview of the ATLAS detector and of the first data collected has already been described in a previous presentation at this conference [2]. Consequently, the aim of this contribution is to highlight a few of the early physics processes which are attainable with the first few nb^{-1} of integrated luminosity, and to illustrate the related analyses and results obtained to date.

2. RECONSTRUCTION OF UNSTABLE LIGHT HADRONS

Decays of well known light mesons and baryons such as π^0, η, K^0_S, Φ^0 and Λ^0, Ξ, Ω can be used to study fragmentation models that are important for modeling underlying-event dynamics, which in turn are a background to high-p_T processes in hadron-hadron colliders. Since these particles have well known masses and lifetimes, their accurate reconstruction is a powerful data-driven tool for validating the performance of both, the ATLAS detector and the reconstruction algorithms. Early studies [3–5] already provided confidence in the energy scale and resolution of the electromagnetic calorimeter, and the p_T scale and resolution of the Inner Detector at low energies and transverse momenta, respectively. The

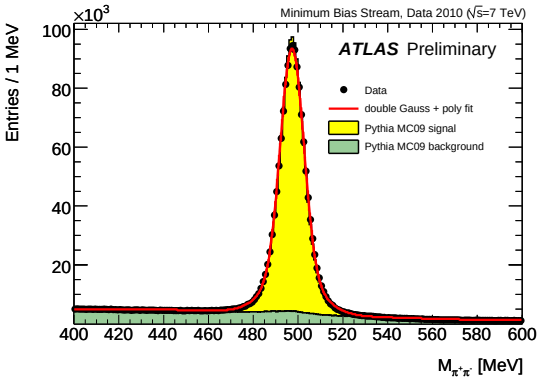

Figure 1. Comparison of the measured and predicted $K^0_S \to \pi^+\pi^-$ invariant mass distribution in the barrel detector region ($|\eta| < 1.2$ for both pion tracks). The signal and background from the simulation have been separately adjusted to match the signal/background ratio observed in the data.

accurate reconstruction of such low energy particles is very sensitive to the material in the Inner Detector, but also to residual mis-alignments and the modeling of the magnetic field. The agreement between data and expectation (from Monte-Carlo simulations) has generally been found to be surprisingly good for a detector that is taking data for the first time. As an example, Fig. 1 shows the observed and expected invariant mass distribution for $K^0_S \to \pi^+\pi^-$ events in the barrel detector region [6]. The mean and resolution of the mass peak obtained from the fit to the data are in excellent agreement with the simulation, with a mass consistent with the PDG value.

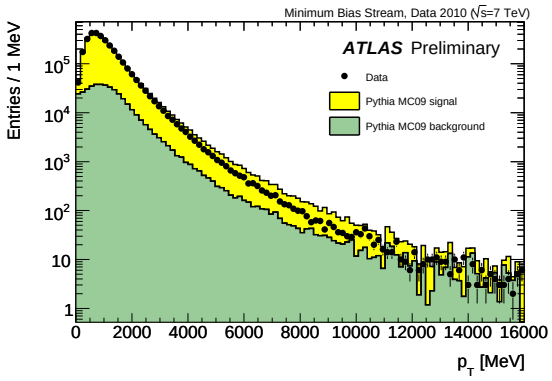

Figure 2. Comparison of the measured and predicted K^0_S transverse momentum distribution in the barrel detector region. The signal and background from the simulation have been separately adjusted, as in Fig. 1.

The study of kinematic variables (e.g. pseudorapidity, transverse momentum, and proper decay time distributions) allow to examine the detector performance in even more detail. The p_T spectrum of K^0_Ss shown in Fig. 2 shows rather good agreement with Monte-Carlo data as well. The simulation appears to overestimate the background at high p_T, an effect which is being studied in the continuing analysis together with acceptance and efficiency corrections.

The more complex cascade decays $\Xi \to \Lambda\pi$, $\Omega \to \Lambda K$, $K^*(892) \to K^0_S\pi$ have also been successfully reconstructed in the first data recorded by the ATLAS experiment in pp collisions at $\sqrt{s} = 7$ TeV [7]. The results demonstrate good performance of the ATLAS track and vertex reconstruction algorithms. When compared to the known masses of these particles, the fitted masses of the observed invariant mass peaks imply the momentum scale to be correct to better than 1%.

3. INNER DETECTOR TOMOGRAPHY WITH γ CONVERSIONS

An accurate map of the material in the installed Inner Detector can be directly obtained by reconstructing the secondary vertices of e^+e^- pairs resulting from photon conversions in some piece of material [8]. The spacial distribution of such vertices yields precise tomographic images of the material in the Inner Detector, such as the one shown in Fig. 3. By comparing the radial and longitudinal projections of such distributions with those from Monte-Carlo simulations, it has been possible to discover components which in the geometric model of the detector appear to be displaced with respect to their actual locations in the real detector. More recently, a similar and complementary study reconstructing the vertices of secondary hadronic interactions has also been performed [9]. Any discrepancies between Monte-Carlo and real data found by these studies are being used to correct and further refine the detailed model of the ATLAS detector, which is used in both the simulation and the reconstruction software.

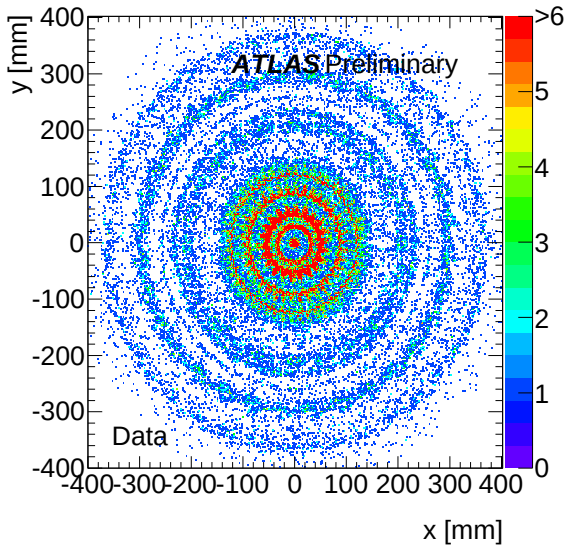

Figure 3. Positions of reconstructed γ conversion vertices projected onto the transverse plane. The beam pipe, the three pixel barrel layers, the pixel support structure, and the first two barrel layers of the Silicon Strip Tracker (SCT) are visible. The spot in the center of the beam pipe is due to Dalitz decays, $\pi^0 \to \gamma e^+e^-$.

4. HEAVY FLAVOUR

The production of charm and beauty mesons are among the first hard processes that are observable at the LHC. Clear signals from the decays of $D^{*\pm}$, $D^{\pm}$ and $D_s^{\pm}$ mesons have been observed by ATLAS in pp collisions at $\sqrt{s} = 7$ TeV already with $\sim$1.4 nb^{-1} of integrated luminosity [10].

$J/\psi \to e^+e^-$ and $J/\psi \to \mu^+\mu^-$ signals were first reported for integrated luminosities of $\sim$6.3 nb^{-1} and $\sim$6.4 nb^{-1}, respectively. Precise measurements of J/ψ properties in ATLAS form a crucial step both for understanding the detector performance and for performing measurements of various B-physics channels. Furthermore, J/ψ production cross-section measurements at LHC will provide sensitive tests of QCD predictions.

Di-muons from $J/\psi \to \mu^+\mu^-$ decays provide an excellent testing ground for studies of muon trigger and identification efficiencies, as well as the momentum scale and resolution of muons with transverse momentum below 20 GeV (the low $p_{\rm T}$ region). Muon identification and reconstruction extend to $|\eta| < 2.7$, covering a $p_{\rm T}$ range from 1 GeV to around 1 TeV.

In the initial $J/\psi \to \mu^+\mu^-$ analysis [11], one of the two muons was required to be a *combined* muon, characterized by tightly matched tracks from the Inner Detector and from the Muon Spectrometer. The second muon could be either a combined or a *tagged* muon, where the latter is characterized by an Inner Detector track with an extrapolation pointing to a track segment in the Muon Spectrometer. Combined muons are limited to the pseudo-rapidity range $|\eta| < 2.5$, and tagged muons to $|\eta| < 2.0$.

Because of the low momentum of the muons, which on average suffer an energy loss of ~ 3 GeV in the calorimeters, only the track parameters from the Inner Detector were used to evaluate the invariant mass in this analysis. The mass spectrum is shown in Fig. 4, and the quantitative results of this early analysis are summarized in Table 1.

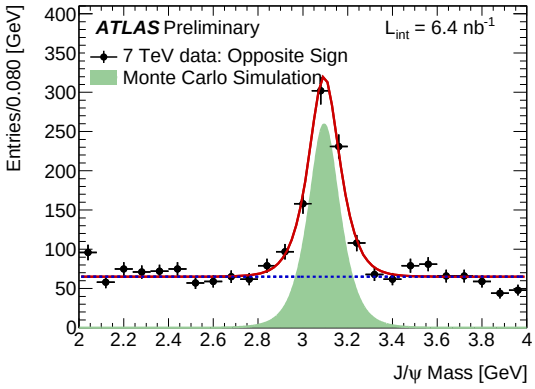

Figure 4. Invariant mass distribution of reconstructed $J/\psi \to \mu^+\mu^-$ candidates. The solid line is the result of an unbinned maximum likelihood fit to all di-muon pairs in the mass window $2-4$ GeV, and the dashed line is the fit result for the background. The green solid area represents the prompt J/ψ MC normalised to the number of signal events obtained from the fit.

Table 1
Results of the unbinned likelihood fit to the invariant masses of $J/\psi \to \mu^+\mu^-$ candidates. The number of background events is given in the range $m_{J/\psi} \pm 3\sigma_m$. The statistics corresponds to 6.4 ± 1.3 nb^{-1} of integrated luminosity at $\sqrt{s} = 7$ TeV.

$m_{J/\psi}$ [GeV]	3.095 ± 0.004 (stat)
signal	612 ± 34 events
background	332 ± 9 events

5. CHARGED PARTICLE MULTIPLICITIES

In the first ATLAS measurements of charged particle distributions at $\sqrt{s} = 7$ and 0.9 TeV [12,13], it was found that while the agreement between data and the PYTHIA Monte-Carlo tune ATLAS MC09c [14] was good in most distributions, deviations occurred in the transverse momentum spectrum in the region $p_{\rm T} > 3$ GeV, and in the charged particle multiplicity distribution for $n_{ch} > 40$.

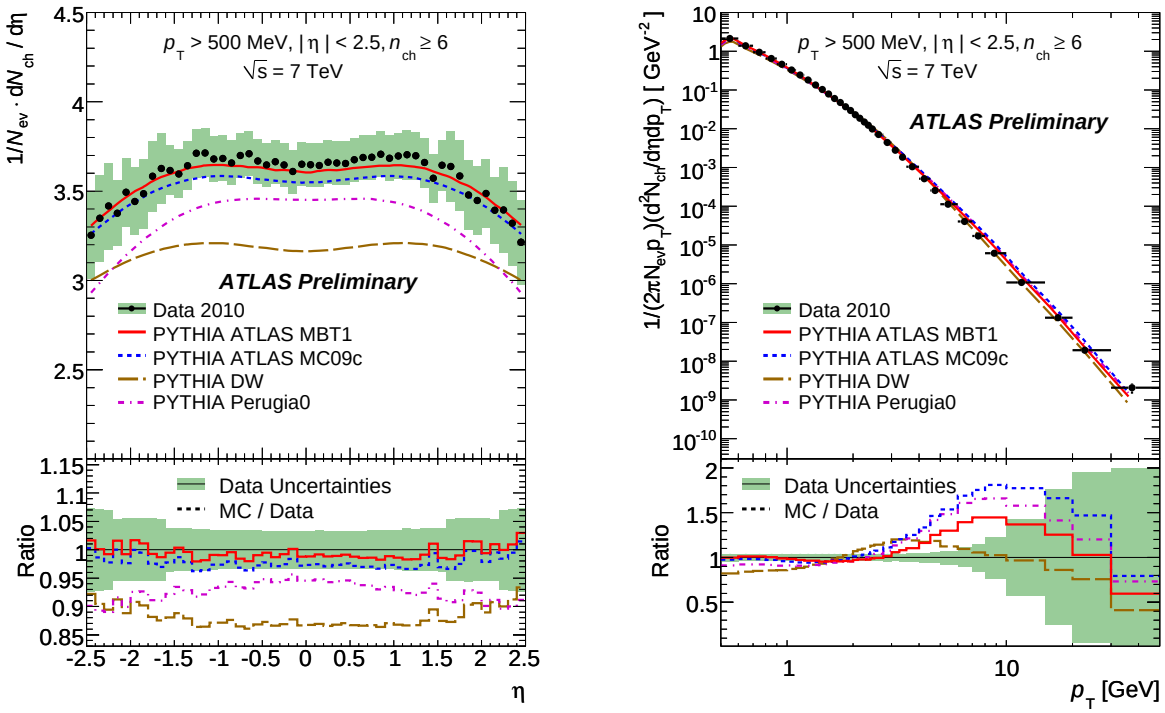

(a) (b)

Figure 5. Charged-particle multiplicity as a function of pseudo-rapidity (a) and transverse momentum (b) at $\sqrt{s} = 7$ TeV for events with $n_{ch} \geq 6$ within the kinematic range $p_{\mathrm{T}} > 500$ MeV and $|\eta| < 2.5$. The dots represent the data and the curves the predictions from different Monte Carlo models. The vertical bars represent the statistical uncertainties, while the shaded areas show statistical and systematic uncertainties added in quadrature. The values of the ratio histograms refer to the bin centroids.

Events selected by the scintillator-based single-arm minimum-bias trigger (MBTS) include contributions from diffractive processes, which make it difficult to compare the data with non-diffractive Monte Carlo (MC) models. In the analysis of ref. [15], the phase space was therefore restricted to $n_{ch} \geq 6$ charged particles in order to eliminate diffractive events. The data were then compared to various existing MC models tuned on minimum bias data from $\sqrt{s} = 1.96$ TeV $p\bar{p}$ collisions at the Tevatron. The ATLAS data sample was also used for a new tuning of PYTHIA6 to LHC data at $\sqrt{s} = 900$ GeV and $\sqrt{s} = 7$ TeV, called ATLAS MBT1 (ATLAS Minimum Bias Tune 1). This tune improved the modeling of the p_{T} and n_{ch} spectra observed in the ATLAS detector, which is important for correctly predicting the background to be expected at nominal LHC luminosity with many interactions per bunch crossing (pileup).

In Fig. 5(a) the charged particle multiplicity at $\sqrt{s} = 7$ TeV in events with $n_{ch} \geq 6$ is shown as a function of pseudo-rapidity and compared to various MC tunes. The same is shown in Fig. 5(b) as a function of transverse momentum. It can be seen that the new tune ATLAS MBT1 comes closest to the data (the Perugia0 tune fails to describe the low-p_{T} region), but still overshoots the data in the range $4 \leq p_{\mathrm{T}} \leq 10$ GeV.

The angular distribution of charged particles with respect to the leading particle (defined by the highest-p_{T} track), as well as the correlation

between mean transverse momentum and charged particle multiplicity, were studied in ref. [16]. These observables are sensitive to the characteristics of the underlying event. A higher underlying event activity was seen in the data than that predicted by various Monte Carlo tunes.

6. INCLUSIVE JET PROPERTIES AT $\sqrt{s} = 7$ TeV

The production of energetic jets of particles in proton-proton collisions constitutes a fundamental prediction of QCD and a distinctive signature of short-distance (hard) interactions between partons, leading to collimated flows of hadrons at high transverse momentum in the final state. The study of particle jets began in ATLAS already in December 2009, with data from pp collisions collected at 900 GeV centre-of-mass energy [17–19].

In the more recent data of $1\,\mathrm{nb}^{-1}$ integrated luminosity collected at 7 TeV collision energy, events with up to 6 jets in the final state and p_{T}^{jet} up to ~ 500 GeV were observed [20]. Jets are searched for using the anti$-\mathrm{k_T}$ jet algorithm with $\mathrm{R} = 0.6$, four-momentum recombination, and the energy depositions in calorimeter clusters as input. Topological clusters are built around seed calorimeter cells with $|E_{\mathrm{cell}}| > 4\sigma$ of the noise, to which all directly neighbouring cells are added. Further neighbours of neighbours are iteratively added for all cells with signals above a secondary threshold $|E_{\mathrm{cell}}| > 2\sigma$, where σ is defined as the RMS of the cell energy noise distribution.

In ref. [20], different jet kinematic distributions in inclusive jet and dijet production are studied, as well as the internal jet structure and the charged particle flow in the event, confirming the notion of collimated flows of particles in the direction of a jet. The data are compared to Monte Carlo simulations based on perturbative leading-order QCD plus parton shower predictions, with a full simulation of the ATLAS detector response. Figure 6(a) shows the observed distribution of the jet rapidity, y^{jet}, for all jets with $p_{\mathrm{T}}^{jet} > 30$ GeV and $|y^{jet}| < 2.8$ in the final state. No corrections for detector effects were applied, and only statistical errors are shown. The Monte Carlo simulated events provide a reasonable description of

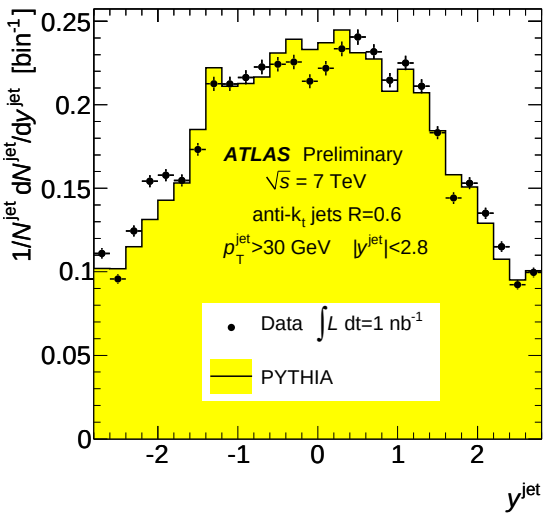

(a) Observed inclusive jet rapidity distribution.

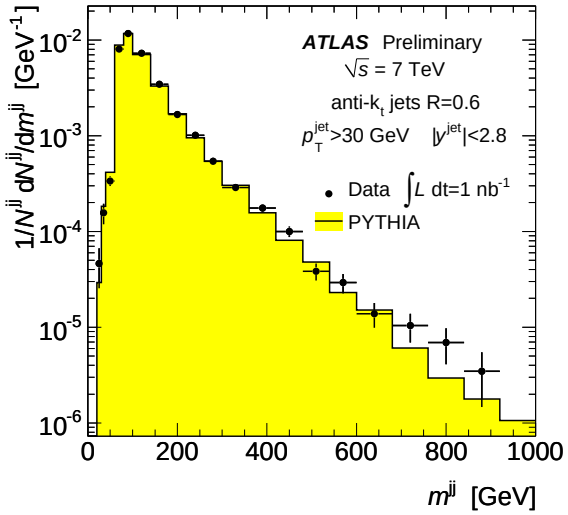

(b) Observed m_{jj} distribution in inclusive dijet events.

Figure 6. Observed inclusive jet rapidity and inclusive dijet mass distributions for jets with $p_{\mathrm{T}}^{jet} > 30$ GeV and $|y^{jet}| < 2.8$. Only statistical uncertainties are included and the distributions are normalized. The data (black dots) are compared to PYTHIA Monte Carlo predictions (yellow histograms).

the data, albeit a few discrepancies which are undergoing further scrutiny.

In about 20% of the events which contain at least one jet with $p_{\mathrm{T}}^{jet} > 30$ GeV and $|y^{jet}| < 2.8$, one or more additional jets are found that satisfy the same criteria. The azimuthal angular separation $|\Delta\phi^{\mathrm{jj}}|$ of the two leading jets exhibits a prominent peak at $|\Delta\phi^{\mathrm{jj}}| = \pi$, indicating a dominant back-to-back dijet configuration in the final state. The invariant mass m_{jj} of the two leading jets is shown in Fig. 6(b). The shape of the distribution at low m_{jj} is a result of the event selection cuts applied on p_{T}^{jet} and $|y^{jet}|$. The data show a decreasing m_{jj} spectrum as m_{jj} increases from 50 GeV to about 1 TeV, as expected and correctly predicted by the Monte Carlo simulation.

7. W AND Z BOSONS

The W and Z bosons are expected to be produced abundantly at the LHC, and for the first time in proton-proton collisions. The high LHC energy will allow for detailed measurements of their production properties at a previously unexplored energy scale. These conditions will provide new insights on the proton properties, tests of perturbative QCD, and ultimately a precise determination of the mass of the W boson. In this process, the well-known Z boson will serve as a precise yardstick for the determination of the detector performance: its known mass, width and leptonic decays can be exploited to measure precisely the detector energy and momentum scale, resolution, as well as lepton identification and trigger efficiencies.

The critical first step in making such precision measurements is to observe W and Z production in the $\sqrt{s} = 7$ TeV pp collisions of the LHC. The ATLAS experiment observed its first events in a seven-week period from March to May 2010, namely 17 $W \to e\nu$ and 40 $W \to \mu\nu$ candidates resulting from total integrated luminosities of $6.7\,\mathrm{nb}^{-1}$ and $6.4\,\mathrm{nb}^{-1}$ in the electron and muon channels, respectively [21]. One $Z \to ee$ and two $Z \to \mu\mu$ candidates were also found with data corresponding to integrated luminosities of $6.7\,\mathrm{nb}^{-1}$ and $7.9\,\mathrm{nb}^{-1}$, respectively. The uncertainty on the luminosity determination is on the order of 20%. The statistics is summarized in Table 2, including expected background contributions. Full details of the analysis with a discussion of the systematic uncertainties are given in ref. [21].

Table 2
Statistics of the first observation by the ATLAS experiment of W and Z production in $\sqrt{s} = 7$ TeV pp collisions at the LHC.

Channel	$W \to$		$Z \to$	
	$e\nu$	$\mu\nu$	ee	$\mu\mu$
Observed	17	40	1	2
Expected	23	29	1.6	3.2
signal	21	26	1.6	3.2
background	2	3		
$\mathscr{L}$ [nb^{-1}] ($\pm$20%)	6.7	6.4	6.7	7.9

8. SUMMARY

The ATLAS detector has shown excellent performance in the first few months of collecting data from $\sqrt{s} = 900$ GeV and $\sqrt{s} = 7$ TeV proton-proton collisions delivered by the LHC — a great reward for the many long years of design, construction and commissioning of the experiment. The detector is generally well described by Monte Carlo simulations, and the detector response is already remarkably well understood. Detailed comparisons of data and simulations will obviously be continued and, with more statistics, lead to a very precise description of the detector and its performance.

The rapid turn-on of the LHC has allowed ATLAS to rediscover most of the Standard Model particle spectrum already. In this short writeup only few could be covered, though many more have been presented at this and other conferences.

While the ATLAS Collaboration is publishing its first results, data taking continues with the LHC ramping up in performance at a formidable pace — almost doubling the integrated luminosity every week. The results presented here will therefore be long out-dated by the time these proceed-

ings are assembled and go to print. Nevertheless, may they serve as a reference for the rapid and highly successful turn-on of the LHC and its experiments.

REFERENCES

1. The ATLAS Collaboration, *Performance of the ATLAS Detector using First Collision Data* , submitted to JINST (2010), arXiv:1005.5254 [hep-ex].
2. L. Rossi on behalf of the ATLAS Collaboration, *ATLAS Status*, these proceedings.
3. The ATLAS Collaboration, *Performance of the ATLAS electromagnetic calorimeter for* $\pi^0 \to \gamma\gamma$ *and* $\eta \to \gamma\gamma$ *events* , ATLAS-CONF-2010-006.
4. The ATLAS Collaboration, *Estimating Track Momentum Resolution in Minimum Bias Events using Simulation and* K^0_S *in* $\sqrt{s} = 900$ GeV *collision data*, ATLAS-CONF-2010-009.
5. The ATLAS Collaboration, *Study of the Material Budget in the ATLAS Inner Detector with* K^0_S *decays in collision data at* $\sqrt{s}$*= 900 GeV*, ATLAS-CONF-2010-019.
6. The ATLAS Collaboration, *Kinematic Distributions of* K^0_S *and* Λ *decays in collision data at* $\sqrt{s}$ *= 7 TeV*, ATLAS-CONF-2010-033.
7. The ATLAS Collaboration, *Observation of* Ξ*,* Ω *baryons and* $K^*(892)$ *meson production at* $\sqrt{s} = 7$ TeV , ATLAS-CONF-2010-032.
8. The ATLAS Collaboration, *Photon Conversions at* $\sqrt{s} = 900$ GeV *measured with the ATLAS Detector*, ATLAS-CONF-2010-007.
9. The ATLAS Collaboration, *Mapping the material in the ATLAS Inner Detector using secondary hadronic interaction in* 7 TeV *collisions*, ATLAS-CONF-2010-058.
10. The ATLAS Collaboration, *D* mesons reconstruction in pp collisions at* $\sqrt{s}$ *= 7 TeV*, ATLAS-CONF-2010-034.
11. The ATLAS Collaboration, *First observation of the* $J/\psi \to \mu^+\mu^-$*resonance in ATLAS pp collisions at* $\sqrt{s} = 7$ TeV, ATLAS-CONF-2010-045.
12. The ATLAS Collaboration, *Charged-particle multiplicities in pp interactions at* $\sqrt{s} = 900$ GeV *measured with the ATLAS detector at the LHC*, Phys. Lett. **B688** (2010) 2142, arXiv:1003.3124 [hep-ex].
13. The ATLAS Collaboration, *Charged-particle multiplicities in pp interactions at* $\sqrt{s} = 7$ TeV *measured with the ATLAS detector at the LHC*, ATLAS-CONF-2010-024.
14. T. Sjostrand, S. Mrenna, and P. Skands, *PYTHIA 6.4 physics and manual*, JHEP **05** (2006) 026, hep-ph/0603175.
15. The ATLAS Collaboration, *Charged particle multiplicities in pp interactions at* $\sqrt{s} = 0.9$ *and* 7 TeV *in a diffractive limited phase space measured with the ATLASdetector at the LHC and a new* PYTHIA6 *tune*, ATLAS-CONF-2010-031.
16. The ATLAS Collaboration, *Track-based underlying event measurements in pp collisions at* $\sqrt{s} = 900$ GeV *and* 7 TeV *with the ATLAS Detector at the LHC*, ATLAS-CONF-2010-029.
17. The ATLAS Collaboration, *Jet kinematic distributions in proton-proton collisions at* $\sqrt{s} = 900$ GeV *with the ATLAS detector*, ATLAS-CONF-2010-001.
18. The ATLAS Collaboration, *Reconstruction of jets from tracks in proton-proton collisions at centre-of-mass energy* $\sqrt{s} = 900$ GeV *with the ATLAS detector*, ATLAS-CONF-2010-002.
19. The ATLAS Collaboration, *Properties and internal structure of jets produced in proton-proton collisions at* $\sqrt{s} = 900$ GeV, ATLAS-CONF-2010-018.
20. The ATLAS Collaboration, *Observation of Energetic Jets in pp Collisions at* $\sqrt{s} = 7$ TeV *using the ATLAS Experiment at the LHC*, ATLAS-CONF-2010-043.
21. The ATLAS Collaboration, *Observation of* $W \to \ell\nu$ *and* $Z \to \ell\ell$ *production in proton-proton collisions at* $\sqrt{s} = 7$ TeV *with the ATLAS detector*, ATLAS-CONF-2010-044.